SUPPORTING INFORMATION

Conceptualising carbon cycling pathways across different land-use types based on rates and ages of soil-respired CO_2

Luisa I. Minich, Dylan Geissbühler, Stefan Tobler, Annegret Udke, Alexander S. Brunmayr, Margaux Moreno Duborgel, Ciriaco McMackin, Lukas Wacker, Philip Gautschi, Negar Haghipour, Markus Egli, Ansgar Kahmen, Jens Leifeld, Timothy I. Eglinton, Frank Hagedorn

Correspondence to: Luisa I. Minich (luisa.minich@gmail.ch)

This file includes Supplement S1 – S7, Table S1 – Table S7, Figure S1 – S17.

Supplement S1: *In situ* gas sampling procedure for subsequent $^{14}CO_2$ analysis.

After flushing of the chambers, gas samples were collected using a flow-through system connected to a LI-COR gas analyser. Two H_2O traps within the flow-through system prevented moisture from entering the LI-COR pump and air bag during the measurement and sample collection. We first scrubbed all gas tubes, and H_2O traps, with a CO_2 scrubber (soda lime) to remove atmospheric background CO_2 in the flow-through system. The flow-through system, including a 2 L air bag was connected to the first chamber and the air bag was filled to one third with air from the chamber headspace. We stopped the pump and closed the valves of the air bag, as well as of the chamber. We subsequently connected the flow-through system to the second chamber. This approach was repeated for all three chambers. To compensate for the underpressure inside the chamber headspace arising through the sampling, we connected all three chambers with gas tubes, allowing air from the other chambers entering the chamber that was sampled. The $^{14}CO_2$ sampling scheme is presented in Figure S1.

Supplement S2: Procedure for gas sampling from root and soil incubations.

For gas sampling from incubations, we attached the bottle to a flow-through system connected to a LI-COR gas analyser. Before the sampling, CO_2 was scrubbed from all gas tubes and H_2O traps using soda lime. If the CO_2 concentration inside the bottle was high enough for ^{14}C analysis (> 2000 ppm), we pumped the air from the bottle through a 2 L air bag which was pre-filled with synthetic air to maintain the pressure inside the flow-through system. We stopped the pump and closed the valves of the air bag when the air from the bottle and 2 L air bag was thoroughly mixed within the system (i.e. CO_2 concentration remained constant).

Supplement S3: Estimation of ages from $\Delta^{14}CO_2$ signatures with the web-based OxCal software

OxCal is based on Bayesian statistical methods that integrate ^{14}C data with calibration curves to produce calibrated age ranges. The model outputs are probability distributions, typically reported as ranges within a 95.4% confidence interval. These age ranges are expressed in calBP (calibrated years before 1950). Ages reported in this study are related to the sampling date (i.e., calBP + (2023-1950)). We generally focused on the age ranges with the highest probability within the given confidence interval. However, most plausible ranges were chosen in consideration of a reasonable depth function. For instance, if the $\Delta^{14}C$ value of CO_2 respired from topsoil was higher than from subsoil, we interpreted the $\Delta^{14}CO_2$ from subsoil to reflect older ages (on the pre-peak side of the bomb curve), although the more depleted $\Delta^{14}C$ value could also indicate more modern levels than for topsoil. To account for the greater dilution of atmospheric $^{14}CO_2$ observed at our sites compared to the Jungfraujoch station, we adjusted the bomb curve for each site. This adjustment was made by subtracting the mean seasonal difference (summer and winter) between our site-specific observations and the original bomb curve data, assuming a consistent offset from 1951 to 2024. For modern samples, the age was determined by comparing the respired $\Delta^{14}CO_2$ with site-specific bomb curve $\Delta^{14}CO_2$ values. The age was deduced by identifying the year on the bomb curve with the smallest error between the respired and atmospheric $\Delta^{14}CO_2$.

Supplement S4: Constraints and modification of input data of Bayesian mixing models.

Partitioning of sources of *in situ* soil respiration in winter is constrained by deviations of soil water contents between summer and winter. Soils that we sampled during the summer campaign were incubated at field-moist conditions which likely deviated from conditions in winter. Respiration rates from each depth layer were likely also driven by soil water contents. Since we did not repeat the soil sampling and incubations for the winter campaign, we were not able to account for seasonal differences in respiration rates derived from changes in soil water contents.

We modified or supplemented input data of Bayesian mixing models in case original data would have resulted in implausible results. Following changes were conducted:

(i) For two sites (Altwi, Underi Site with mineral soil coverage), we observed unrealistically depleted $\Delta^{14}CO_2$ values (< -100 ‰) of atmospheric background, likely deriving from fossil contamination. In these cases, we used atmospheric $\Delta^{14}CO_2$ values of the site with closest proximity (i.e. Reckenholz, Underi Site original, respectively).

(ii) Root incubations were not conducted for all sites in winter. For sites for which we conducted root incubations (Figure S2), we calculated the mean difference between $\Delta^{14}CO_2$ values of atmospheric background and autotrophic respiration. We added this mean value to the atmospheric background $\Delta^{14}CO_2$ for the sites for which we did not conduct root incubations and took the resulting $\Delta^{14}CO_2$ value as endmember value for autotrophic respiration. For $\delta^{13}CO_2$, we used values derived in summer for the respective depths.

Supplement S5: Overcoming limitations of MixSIAR using a Python-based alternative.

We used the Bayesian mixing model MixSIAR because it is an established tool for estimating source proportions. MixSIAR and predecessor versions (SIAR, MixSIR) have been widely and successfully applied to partition sources in ecological research, including autotrophic and heterotrophic sources to soil and ecosystem respiration (Guidi et al., 2023; Hicks Pries et al., 2013, 2015, 2016; Moore & Semmens, 2008; Parnell et al., 2010; Stock et al., 2018). However, MixSIAR has limitations, particularly when dealing with complex source structures.

One key limitation is that MixSIAR's ability to resolve >7 sources using signatures from only two isotopes can result in imprecise model outputs (Stock et al., 2018). Since our incubation experiments included several depth layers—sometimes exceeding 7 sources—we aggregated isotopic signatures from specific depth layers into topsoil and subsoil categories in MixSIAR. This aggregation was based on weighted respiration rates of each depth layer. However, a major drawback of this approach is that it does not allow for incorporating uncertainty in the weighted respiration rates. Additionally, we sought to inform the model about the relative contributions of each depth layer (based on respiration rates) to total heterotrophic respiration to improve the accuracy of estimated source contributions across depth intervals. In MixSIAR, we implemented depth interval contributions (topsoil and subsoil) as informative priors, which constrain parameter estimates and influence parameter estimation (Moore & Semmens, 2008; Stock et al., 2018). However, these informative priors were only applied to heterotrophic respiration (topsoil vs. subsoil), while we lacked information on the contributions of autotrophic and atmospheric sources. To maintain an uninformative prior for these sources, we used $\alpha = (1, 1, 1)$ when assuming three sources: atmosphere, autotrophic respiration, and total heterotrophic respiration (sum of topsoil and subsoil contributions). For example, if topsoil contributed 80% and subsoil 20% to total heterotrophic respiration, the informative prior was set to $\alpha = (1, 1, 0.8, 0.2)$ for the sources: atmosphere, autotrophic, heterotrophic topsoil, and heterotrophic subsoil. However, this approach did not allow for integrating uncertainty in the contribution of depth intervals, introducing the risk of biasing the results due to prior influence. Another limitation of MixSIAR is its reliance on JAGS (Just Another Gibbs Sampler) for Bayesian inference. While JAGS is widely used and relatively easy to set up, it struggles with high-dimensional models and many sources, often resulting in slow convergence and high autocorrelation (Beraha et al., 2021; Bølstad, 2019; Hoffman & Gelman, 2014).

To overcome these limitations, we implemented an alternative Bayesian mixing model in Python using the No-U-Turn Sampler (NUTS). Unlike JAGS, NUTS is more efficient for high-dimensional models, as it uses Hamiltonian Monte Carlo (HMC) to explore the posterior distribution more effectively (Hoffman & Gelman, 2014). This approach allowed us to retain all depth layers as separate sources instead of aggregating them into topsoil and subsoil. In addition, we incorporated weighted respiration rates of each depth layer as deterministic predictors rather than using informative priors. Unlike informative priors, which encode prior knowledge and constrain parameter estimates, deterministic predictors are known variables that directly influence the model (Gelman et al., 2013). In our case, respiration rates of depth layers were used as deterministic predictors to explain variation in mixing proportions without introducing subjective prior assumptions. This approach prevents over-reliance on priors and ensures that source contributions are data-driven rather than prior-constrained (Gelman et al., 2013). Additionally, because NUTS efficiently handles correlated parameters and complex posterior distributions, it reduces autocorrelation and improves convergence speed, making it more suitable for our study where multiple sources contribute to respiration (Hoffman & Gelman, 2014).

For the final results, we combined both model outputs from MixSIAR (JAGS-based) and Python (NUTS-based) by averaging them. This approach increased robustness by reducing reliance on a single model and mitigating potential biases. In cases where both models yielded similar results, this cross-validation strengthened confidence in the estimates. In cases where there was divergence, the averaging of the output helped balancing potential over- or underestimations from each model, ensuring a more reliable estimate. Additionally, MixSIAR offers stability and comparability with existing literature, while the implementation in Python excels in handling a higher number of sources. By averaging the results, we benefit from the strengths of both models and address the differences in assumptions, priors, and implementation choices, ensuring more reliable and generalizable estimates.

Supplement S6: Spatial heterogeneity in $\Delta^{14}C$ signatures of *in situ* soil respired CO_2 and its source contribution

To gain information on spatial heterogeneity of *in situ* soil respired $\Delta^{14}CO_2$ and its source contribution, we repeated respiration rate measurements and gas sampling at three spatially distinct locations at the two forest sites Hölstein and Pfynwald during the winter sampling campaign. In Hölstein, *in situ* soil respired $\Delta^{14}CO_2$ ranged from -5 to 5 ‰ ($\sigma = 5$) and the relative source contribution of heterotrophic respiration from 44 to 62 % ($\sigma = 9$). In Pfynwald, *in situ* soil respired $\Delta^{14}CO_2$ ranged from -6 to 10 ‰ ($\sigma = 9$) and the relative source contribution of heterotrophic respiration from 33 to 73 % ($\sigma = 22$; Figure S16). We assume forests to exhibit higher spatial variability in soil respired $\Delta^{14}CO_2$ and its source contribution than other land-use types due to a higher diversity in the vegetation.

Supplement S7: Effect of carbonate rock weathering on isotopic signatures of heterotrophic respiration

The heterotrophic isotopic signatures ($\Delta^{14}CO_2$, $\delta^{13}CO_2$) of some sites (predominantly croplands), and some soil depths (Table S3) were affected by weathering of carbonate rock which was indicated by $\delta^{13}CO_2$ signatures being higher than for SOC and/or, when the $\Delta^{14}CO_2$ values indicated a greater age of respired CO_2 than of SOC, which seemed unreasonable. While we estimated a potential carbonate contribution (Table S3), we were not able to accurately account for the effect of carbonate on the isotopic signatures of heterotrophic respiration given the limited information on endmember isotopic signatures. The effect of carbonate rock weathering was estimated with certain limitations as follows:

(i) We estimated the carbonate contribution as proposed in previous studies e.g., Schindlbacher et al., 2015) using $\delta^{13}C$ values in a simple mixing model, assuming an endmember value of 0 ‰ for carbonate and equal $\delta^{13}C$ values for SOC and respired CO_2 (HR):

$$f_{carbonate} = \frac{\delta^{13}CO_{2_{HR}} - \delta^{13}C_{SOC}}{\delta^{13}C_{carbonate} - \delta^{13}C_{SOC}}$$

However, this approach was not applicable for croplands and peatlands, as the assumption of $SO^{13}C = {}^{13}CO_2$ may not be true due to the effect of C4 plants which exhibit $\delta^{13}C$ values between -9 and -17 ‰ (Krüger et al., 2024). In addition, we cannot rule out the possibility that $\delta^{13}CO_2$ measurements were influenced by the introduction of atmospheric air into the Exetainer® vials used for gas sampling. However, given that we conducted triplicate sampling for ^{13}C analysis and observed a standard deviation of less than 1 ‰ in most cases, this effect appears negligible.

(ii) Due to the caveats associated with the estimation of the contribution of carbonate weathering with $\delta^{13}C$ signatures, we thus estimated a minimum carbonate contribution using $\Delta^{14}C$ values for all cases where CO_2 age > SOC age, assuming an endmember value of -1000 ‰ for carbonate and equal $\Delta^{14}C$ values for SOC and respired CO_2 as:

$$f_{carbonate} = \frac{\Delta^{14}CO_{2_{HR}} - \Delta^{14}C_{SOC}}{10} \div 100$$

For which the $\Delta^{14}CO_2$ value would shift by -10 ‰ with 1 % carbonate contribution. However, the assumption that $SO^{14}C = {}^{14}CO_2$ is likely incorrect in most cases as the respired CO_2 represents the most labile and youngest fraction of SOC, so that CO_2 age ≤ SOC age. Since we do not have information on isotopic signatures of the respired SOC fraction, we were only able to broadly estimate a potential $\Delta^{14}CO_2$ value by applying the same proportion of $\Delta^{14}CO_2$ to $\Delta^{14}C$ of SOC as calculated from sites of the same land-use type, not affected by carbonate. We then calculated the difference between the measured $\Delta^{14}CO_2$ value and potential $\Delta^{14}CO_2$ value and applied the equation above.

(iii) Finally, we estimated a new $\Delta^{14}CO_2$ value (HR_{corr}), corrected for the effect of carbonate weathering, using the mean value of carbonate contribution calculated from the three approaches above (Table S3):

$$\Delta^{14}CO_{2_{HR_{corr}}} = \frac{\Delta^{14}CO_{2_{HR}} - \Delta^{14}C_{carbonate} \times f_{carbonate}}{1 - f_{carbonate}}$$

Some of the corrected $\Delta^{14}CO_2$ values appear unrealistically high. This could be due to an overestimation of the carbonate contribution and/or use of an $\Delta^{14}C$ endmember assumption of -1000 ‰ for carbonate. During carbonate weathering in soils, carbonate reacts with soil water and CO_2 (potentially derived from soil respiration or diffused atmospheric air) and dissolves to bicarbonate (HCO_3^-):

$$CaCO_3(calcite) + CO_2 + H_2O \rightarrow Ca^{2+} + 2HCO_3^-$$

HCO_3^- in soil solution thus contains C from carbonate ($\Delta^{14}C$ ~ -1000 ‰), as well as C from soil respiration or atmospheric air ($\Delta^{14}C$ > -1000 ‰). HCO_3^- can in turn dissociate and precipitate to $CaCO_3$ and degas as CO_2 from the soil solution, abiotically contributing to the CO_2 released from soil (Schindlbacher et al., 2015). Since the measured CO_2 was likely influenced by carbonate-derived CO_2 degassing from the soil solution, the $\Delta^{14}C$ of this abiotic CO_2 is expected to be less depleted than -1000 ‰, though the exact value of this endmember remains unknown.

Since we were not able to accurately account for the effect of carbonate in the heterotrophic respiration, we used the isotopic values of heterotrophic respiration for all sites and depths as measured. The estimated mean contributions further revealed that the mean effect of carbonate weathering on total heterotrophic respiration and *in situ* soil respiration was < 5 ± 3 % and < 2 ± 1 %, respectively (Table S3).

Table S1: Site specific information on climate, soil type, and vegetation/crop type.

Land use type	Location					Climate		pH (0-10 cm)	Soil type (WRB classification)	Dominant vegetation / Crop type	
	Ecoregion	Site name	Latitude	Longitude	Elevation [meters a.s.l]	MAP [mm]	MAT [°C]			summer	winter
Grassland											
Temperate	Plateau	Chamau	47.2102	8.4104	393	1134	9.9	6.3	Cambisol/Gleysol	Italian ryegrass, white clover	
	Central Alps	Vaz Muldain	46.6903	9.5196	1200	1040	4.9	7.0	Gleyic Fluvisol	mixed grasses	
	Northern Alps	Jaun	46.6114	7.2727	1500	1712	6.0	5.2	Eutric Cambisol	mixed grasses	
Alpine	Central Alps	Flüelapass	46.7433	9.9632	2320	1622*	0.4**	3.5	-	mixed grasses	
	Central Alps	Büelenhorn	46.6791	9.7793	2340	1622*	-0.1**	6.6	-	mixed grasses	
	Central Alps	Radönt	46.7118	9.9387	2340	1622*	0.4**	3.7	-	mixed grasses	
	Centrial Alps	Schwarzhorn	46.7335	9.9530	2630	1622*	-1.2**	4.0	-	mixed grasses	
Forest											
	Northern Alps	Beatenberg	46.7003	7.7625	1511	1725	4.7	3.1	Podzol	Norway Spruce	
	Central Alps	Pfynwald	46.3031	7.6121	615	575	10.6	6.2	Pararendzina	Scots pine	
	Plateau	Hölstein	47.4381	7.7769	550	1009***	9.0***	5.2	-	European beech, Norway Spruce	
Cropland											
	Plateau	Reckenholz	47.4307	8.5220	440	1050	9.4	5.5	Eutric Gleysol	summer maize	winter wheat
	Plateau	Altwi	47.4386	8.5255	493	1050	9.4	7.4	Calcaric Cambisol	summer maize	winter wheat
	Plateau	Changins	46.3820	6.2389	446	994	10.7	7.1	Calcaric Cambisol	summer maize	winter wheat
Managed peatland											
	Plateau	Lindergut	46.9797	7.0983	430	1030****	10.7*****	7.0	Histosol	mixed grasses	
	Plateau	Rimmerzmatte	47.0117	7.0772	432	1030****	10.7*****	7.0	Histosol	onion	cover grass
	Plateau	Underi Site	47.0245	7.2044	438	1030****	10.7*****	7.1	Histosol	summer maize	

** MAP for alpine sites used from closest MeteoSwiss station: Weissflühhorn (2690 Hm)*

*** MAT for alpine sites used from closest IMIS stations (corresponding to elevation): FLU2 for Flüelapass and Radönt, DAV2 for Büelenhorn, ZNZ2 for Schwarzhorn*

**** MAP and MAT for Hölstein used from closest MeteoSwiss station: Basel-Binningen*

***** MAP for peatlands used from closest MeteoSwiss station: Aarberg*

****** MAT for peatlands used from closest MeteoSwiss station: Neuchatêl*

Table S2: Settings of Bayesian mixing models

	Bayesian mixing model	
	MixSIAR in R	**Python**
Model algorithm	Just Another Gibbs Sampler (JAGS)	No-U-Turn Sampler (NUTS)
Chains	3	4
Iterations	1000000	1000
Draws	3000	2000

Table S3: Estimated contribution of carbonate rock weathering to the isotopic signature of heterotrophically respired CO_2. Carbonate contribution to total heterotrophic respiration was calculated by multiplying the flux-weighted contribution of respective depth layers to the total heterotrophic flux with the carbonate contribution in these depths. Carbonate contribution to *in situ* soil respiration was calculated by multiplying the carbonate contribution to total heterotrophic respiration with the mean source contribution of heterotrophic respiration to total soil respiration as derived from the Bayesian mixing models. We estimated carbonate-corrected $\Delta^{14}CO_2$ values for each depth layer and total heterotrophic respiration using a mass-balance approach and assuming isotopic signatures for carbonate of -1000 ‰ for $\Delta^{14}C$ and of 0 ‰ for $\delta^{13}C$. Note that this value is based on speculative assumptions and likely overestimated as we lacked information on isotopic signatures of biotic (SOC-derived) and abiotic (carbonate-derived) CO_2 sources. For further details see Supplement S5.

Site	Land use type	Depths	Carbonate contribution [%], assumption: $SO^{14}C = {}^{14}CO_2$	Carbonate contribution [%], assumption: SOC age > CO_2 age	Carbonate contribution [%], assumption: $SO^{13}C = {}^{13}CO_2$	Mean carbonate contribution [%]	Carbonate contribution to total heterotrophic respiration [%]	Carbonate contribution to *in situ* soil respiration [%]	Calculated $\Delta^{14}CO_2$ value of total heterotrophic respiration (affected by carbonate) [‰]	Estimated $\Delta^{14}CO_2$ value of total heterotrophic respiration (corrected for carbonate) from mean contribution [‰]
Chamau	temperate grassland	10-20	5.61	4.7	5.0	5.1	6.8	0.6 ± 0.5	-77	-9
Chamau	temperate grassland	20-40			12.4	12.4				
Chamau	temperate grassland	40-90	2.4	13.6	26.5	14.2				
Muldain	temperate grassland	10-20	3.7	5.2	6.2	5.0	3.4	4.4 ± 0.6	-11	24
Muldain	temperate grassland	20-40	2.7	2.5	9.8	5.0				
Muldain	temperate grassland	40-70	1.7	3.3	14.5	6.5				
Jaun	temperate grassland	40-90			17.0	17.0	3.4	1.7 ± 1.0	-8	27
Hölstein	forest	5-10	14.2	10.9	12.7	12.6	2.4	1.4 ± 0.2	-11	14
Hölstein	forest	10-20	16.7	15.1	22.8	18.2				
Pfynwald	forest	10-20			10.0	10.0	1.6	1.2 ± 0.3	20	37
Altwi	cropland	0-5	23.0	24.6		23.8	8.3	0.8 ± 0.7	-110	-29
Altwi	cropland	5-10	2.2	2.5		2.3				
Altwi	cropland	10-20	4.7	5.5		5.1				
Altwi	cropland	20-40	4.7	4.7		4.7				
Changins	cropland	0-5	18.2	19.5		18.9	3.0	0.2 ± 0.2	-81	-53
Changins	cropland	10-20	4.1	4.8		4.5				
Changins	cropland	20-40	5.9	5.9		5.9				
Underi Site	managed peatland	40-90	13.5	17.1		15.3	8.7	2.5 ± 1.5	-297	-268

Table S4: Model output of linear regression (LM) model investigating the relationship between *in situ* soil respiration rates and volumetric water content (VWC) as well as soil temperature. The model was performed across all sites and both seasons.

Response variable	**Model structure**		**Model performance**	**Effect and significance of drivers**								
				VWC			**Soil temperature**			**VWC x Soil temperature**		
		Model type	*AIC*	*Coefficient*	*Std. Error*	*p-value*	*Coefficient*	*Std. Error*	*p-value*	*Coefficient*	*Std. Error*	*p-value*
log Respiration rates	VWC x Soil temperature	LM	43.558	0.293	0.086	**0.002****	0.487	0.094	**0.000*****	0.064	0.086	0.468

*Signif. codes: 0 '***' 0.001 '**' 0.01 '*' 0.05 '.' 0.1 ' ' 1*

Table S5: Model output of ANOVA analysis investigating the variance between rates and $\Delta^{14}CO_2$ values of *in situ* soil respiration, $\Delta^{14}CO_2$ values of heterotrophic respiration, and the rel. contribution of heterotrophic respiration to total soil respiration across land-use types and seasons. We included the study sites as random effects in the linear mixed effect (LME) model to account for site-specific differences arising through confounding factors such as soil physical-chemical properties.

Response variable	**ANOVA structure**		**Model performance**	**Significance of drivers**										
				Land-use type			**Season**			**Land-use type x Season**			**Site (random effect)**	
		Model type	*AIC*	*DenDF*	*F*	*p-value*	*DenDF*	*F*	*p-value*	*DenDF*	*F*	*p-value*	*Std.Dev*	*Std.Dev*
sqrt Respiration rates	LU x Season + (1|Site)	LME	140.74	9.507	2.310	0.133	11.244	23.456	**0.000*****	11.259	3.864	**0.040***	1.765	2.046
log SOC decomposability														
topsoil	LU	LM	12.41	4.000	63.024	**0.000*****								
subsoil	LU	LM	37.94	4.000	8.514	**0.002****								
log $^{14}CO_2$ of soil respiration	LU x Season + (1|Site)	LME	-75.18	11.115	9.784	**0.001****	12.134	21.196	**0.001****	12.135	40.501	**0.000*****	0.042	0.010
$^{14}CO_2$ of soil respiration - without peatlands	LU x Season + (1|Site)	LME	-94.94	9.472	10.387	**0.002****	11.139	4.444	**0.059.**	11.151	0.665	0.534	0.007	0.008
exp $^{14}CO_2$ of heterotrophic respiration	LU	LM	-26.27	4.000	48.134	**0.000*****								
Rel. contribution of heterotrophic respiration	LU x Season + (1|Site)	LME	207.08	11.149	2.870	**0.074.**	9.471	2.675	0.135	9.471	1.136	0.383	9.731	22.236

*Signif. codes: 0 '***' 0.001 '**' 0.01 '*' 0.05 '.' 0.1 ' ' 1*

Table S6: Model output of linear regression (LM) model investigating the relationship between rates and $\Delta^{14}CO_2$ values of *in situ* soil respiration, $\Delta^{14}CO_2$ values of heterotrophic respiration, and the rel. contribution of heterotrophic respiration to total soil respiration and elevation for all grassland sites in summer.

Response variable	**Model structure**		**Model performance**	**Effect and significane of driver**		
				Elevation		
		Model type	*AIC*	*Coefficient*	*Std. Error*	*p-value*
Respiration rates	Elevation	LM	86.334	0.019	0.045	0.688
$^{14}CO_2$ of soil respiration	Elevation	LM	-59.157	0.000	0.000	**0.006****
$^{14}CO_2$ of heterotrophic respiration						
topsoil	Elevation	LM	-33.218	0.000	0.000	**0.056.**
subsoil	Elevation	LM	-24.099	0.000	0.000	0.210
Rel. contribution of heterotrophic respiration	Elevation	LM	67.358	0.004	0.012	0.720

*Signif. codes: 0 '***' 0.001 '**' 0.01 '*' 0.05 '.' 0.1 ' ' 1*

Table S7: Respiration rates, $\Delta^{14}CO_2$ value of total soil respiration and rel. source contribution of heterotrophic respiration of the three replicates and their means at the forest sites Hölstein and Pfynwald.

	Hölstein			Pfynwald		
Replicate	**A**	**B**	**C**	**A**	**B**	**C**
Respiration rate [mg CO_2-C m^{-2} h^{-1}]	108 ± 11	86 ± 22	111 ± 10	78 ± 10	133 ± 9	65 ± 7
$\Delta^{14}CO_2$ value of total soil respiraton [‰]	-1 ± 2	5 ± 2	-5 ± 2	-6 ± 1	8 ± 3	10 ± 3
Rel. source contribution [%]	50 ± 15	62 ± 14	44 ± 14	33 ± 15	68 ± 21	73 ± 23
Mean						
Respiration rate [mg CO_2-C m^{-2} h^{-1}]	102 ± 14			92 ± 37		
$\Delta^{14}CO_2$ value of total soil respiraton [‰]	0 ± 5			4 ± 9		
Rel. source contribution [%]	52 ± 9			58 ± 22		

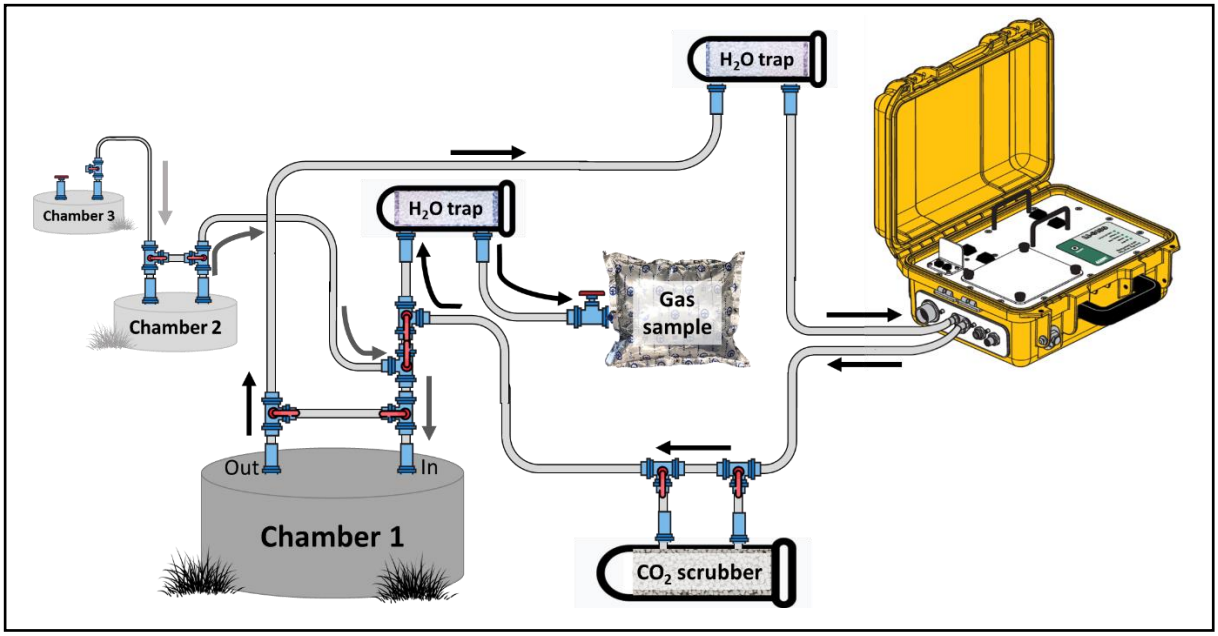

Figure S1: Gas sampling scheme for $^{14}CO_2$ analysis. Connections and valve positions are illustrated in the moment of gas sampling from the chamber headspace. The direction of the red ports indicates closure direction of the valves. For details see Supplement S1. LI-COR icon: credit to LI-COR Environmental.

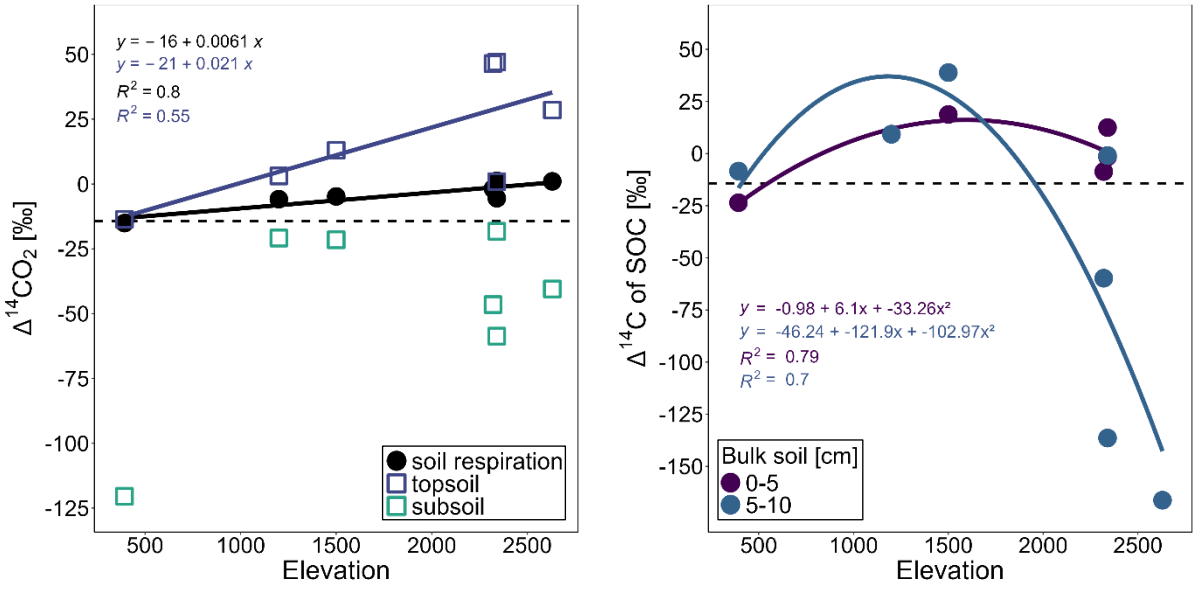

Figure S2: ^{14}C variations in grassland sites with elevation. Left: Variation in summer $\Delta^{14}CO_2$ values (‰) in total soil respiration (black filled circles) and heterotrophic respiration in topsoil (0-10 cm; blue open squares) as well as subsoil (10-90 cm; green open squares). Right: $\Delta^{14}C$ values (‰) of bulk soil SOC in topsoil layers (0-5 cm: purple, 5-10 cm: blue) which follow a polynomial distribution with elevation, being close to modern levels at low elevation, increasing to highest $\Delta^{14}C$ values at elevations of ~ 1500 m and decreasing again for elevations > 1500 m. At highest elevation (> 2000 m), $\Delta^{14}C$ values of soil at 0-5 cm depth remain > 0 ‰, while they sharply decrease in 5-10 cm soil depth to pre-bomb levels. Dashed horizontal lines indicate mean atmospheric background $\Delta^{14}CO_2$ levels across grassland sites in summer.

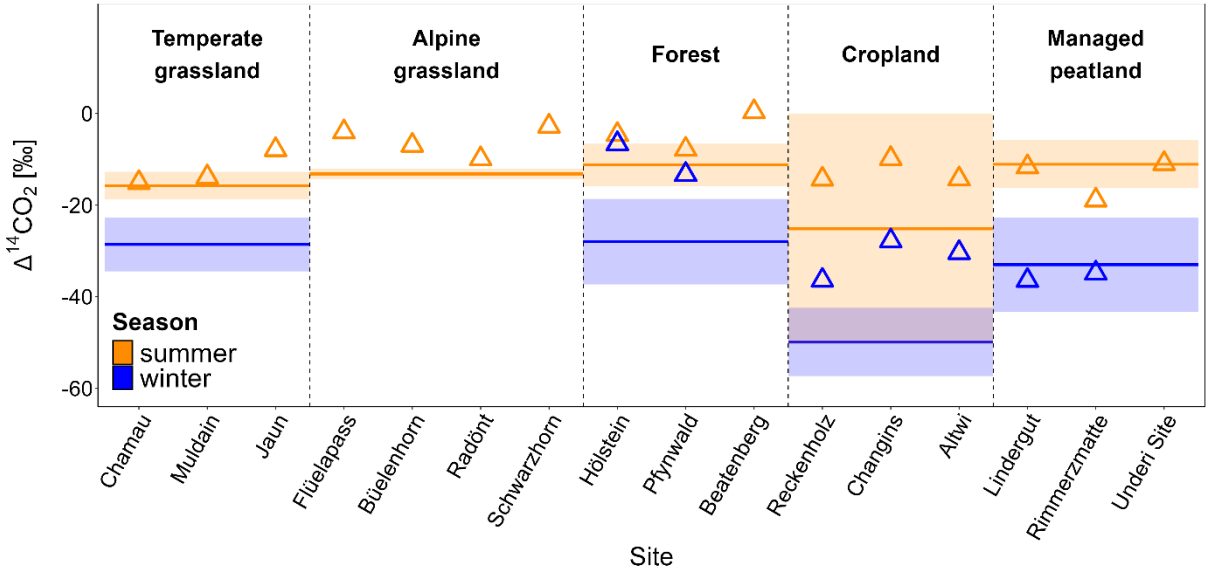

Figure S3: Mean $\Delta^{14}CO_2$ values of atmospheric background for each land-use type (solid line) in summer (orange) and winter (blue) and $\Delta^{14}CO_2$ signatures of autotrophic respiration (open triangles) in summer (orange) and winter (blue).

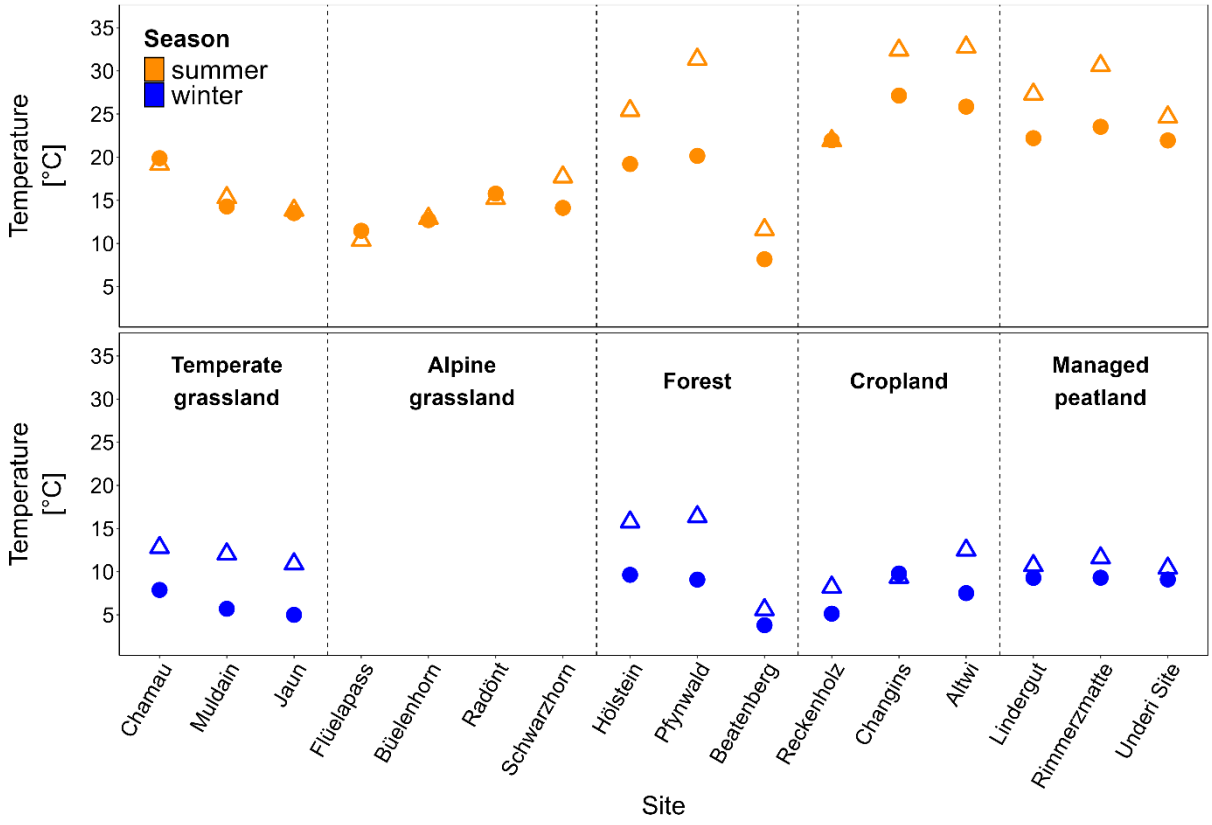

Figure S4: Ambient air temperature (open triangle) and soil temperature (filled circles) in summer (orange) and winter (blue) for each site.

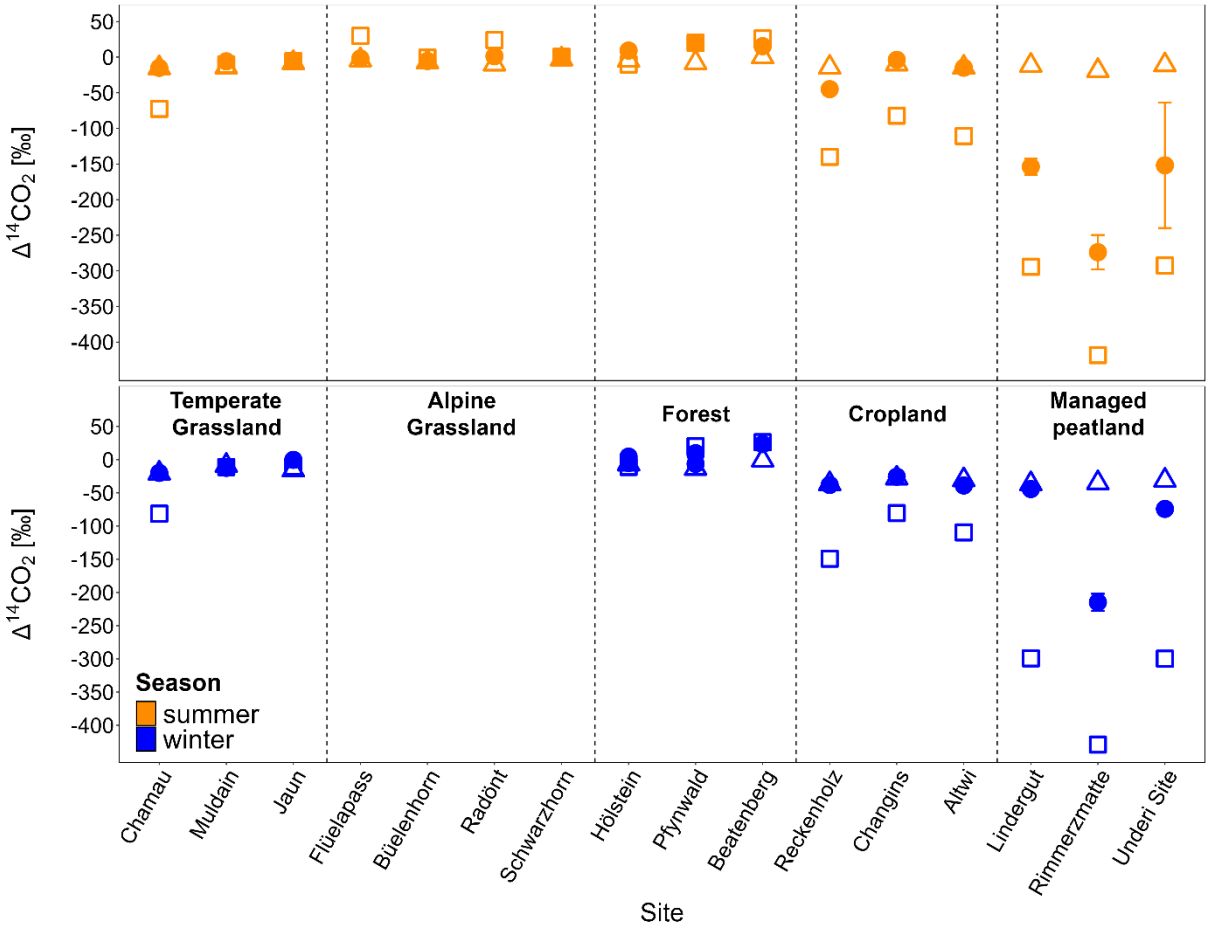

Figure S5: $\Delta^{14}CO_2$ signatures of total soil respiration (filled circles), weighted heterotrophic respiration (open squares) and autotrophic respiration (open triangles) in summer (orange) and winter (blue) for all sites.

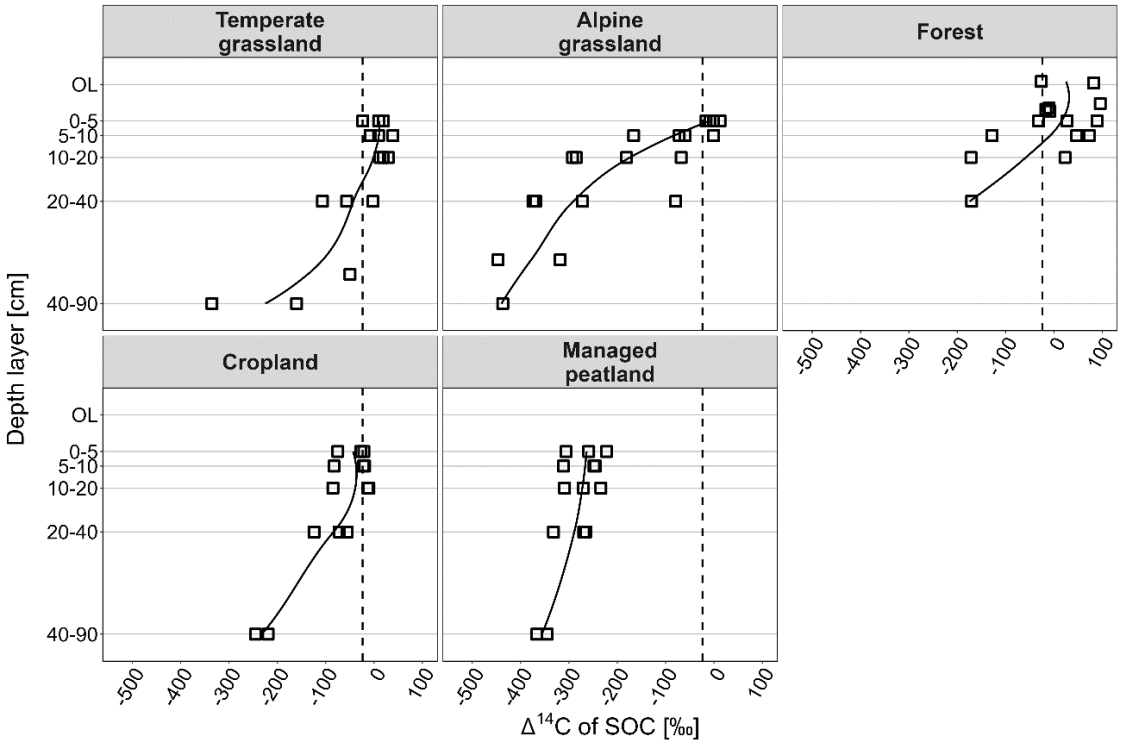

Figure S6: Depth profiles of $\Delta^{14}C$ signatures of SOC in bulk soil across land-use types. OL = organic layer.

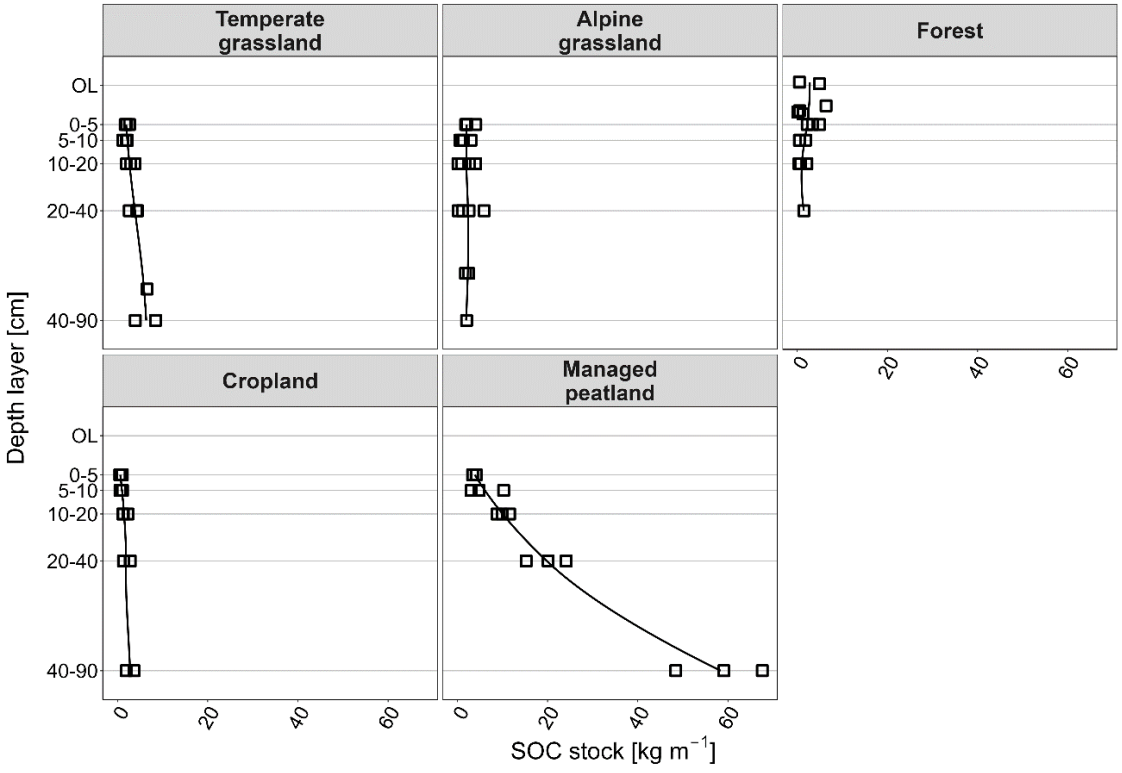

Figure S7: Depth profiles of SOC stocks for each depth layer across land-use types. OL = organic layer.

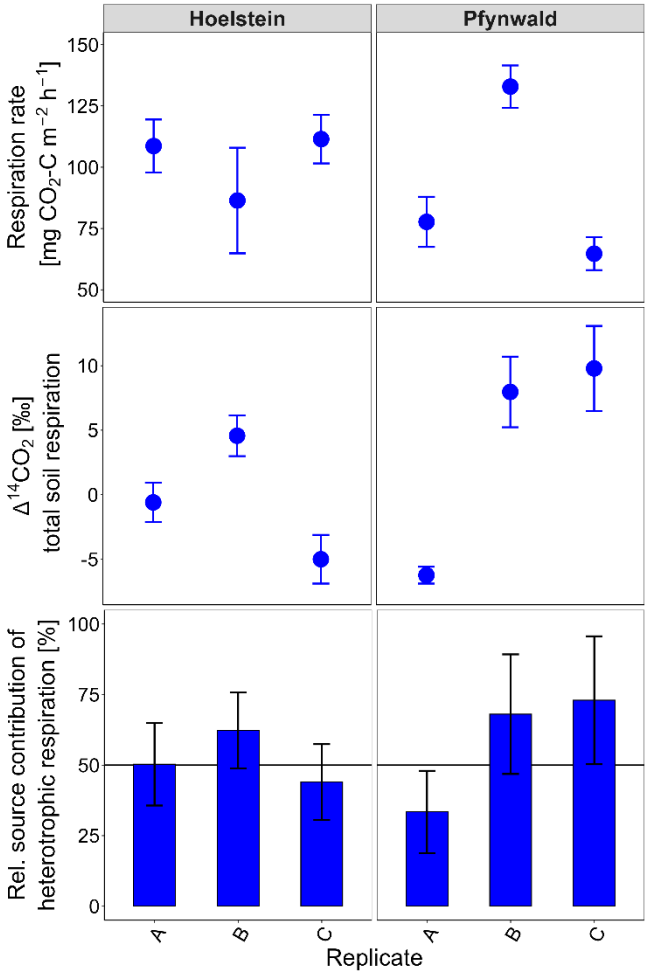

Figure S8: Variation in respiration rate and $\Delta^{14}CO_2$ signature of total soil respiration, as well as rel. source contribution of heterotrophic respiration for winter samples across three spatially replicated measurements and gas samples taken at the forest sites Hölstein and Pfynwald. For details see Supplement S4.

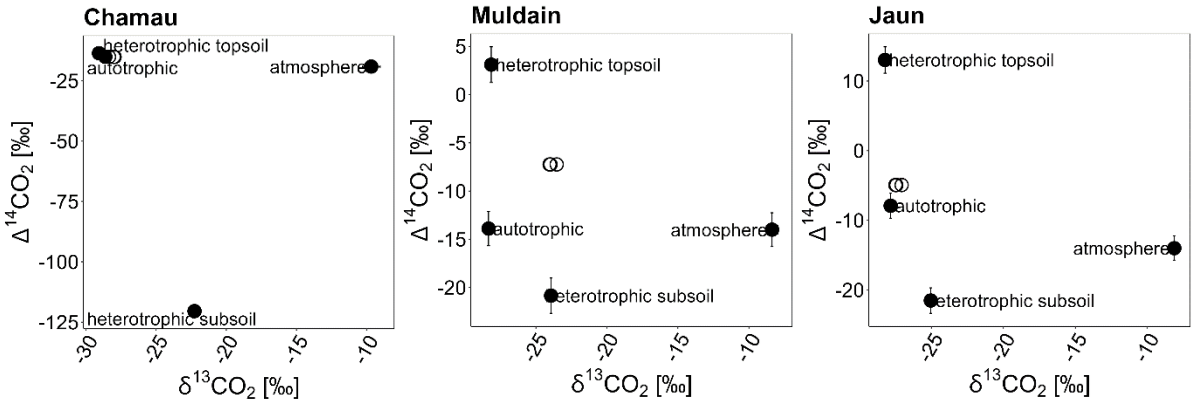

Figure S9: MixSIAR isospace plots for temperate grasslands in summer.

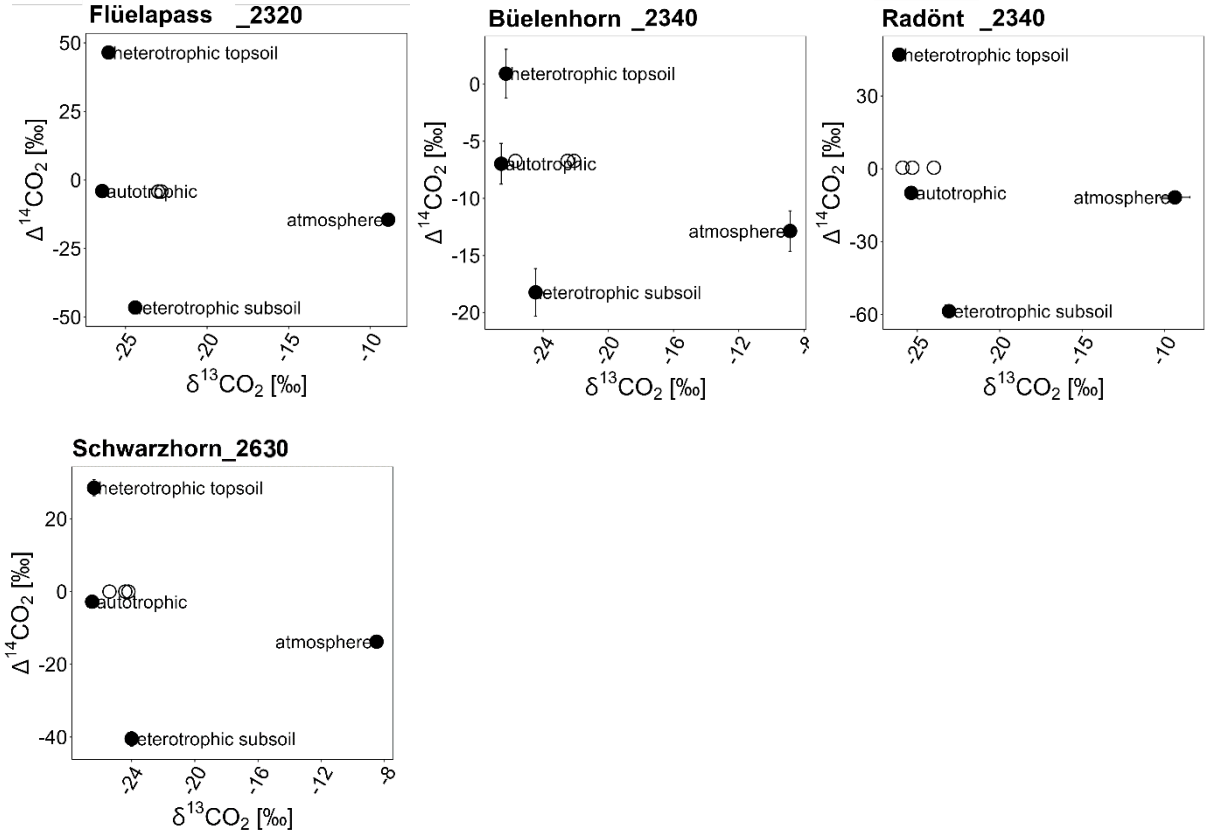

Figure S10: MixSIAR isospace plots for alpine grasslands in summer.

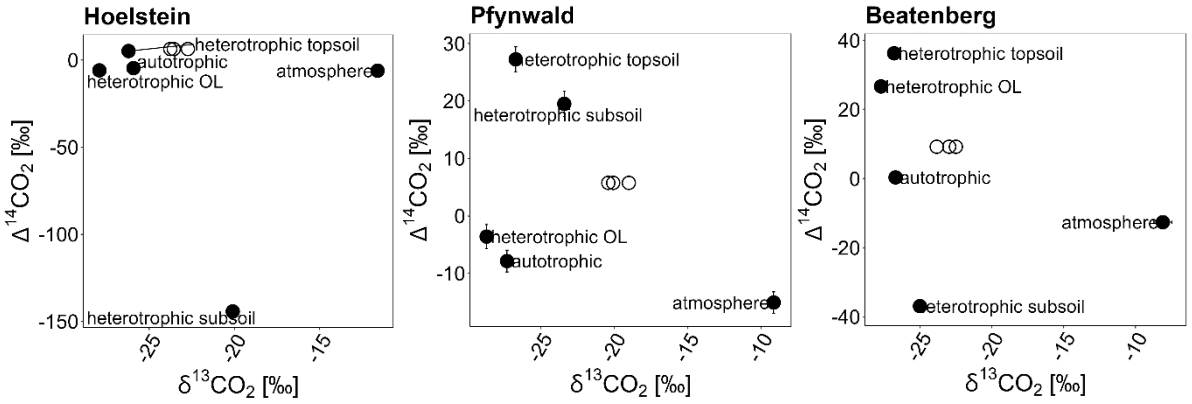

Figure S11: MixSIAR isospace plots for forests in summer. OL = organic layer.

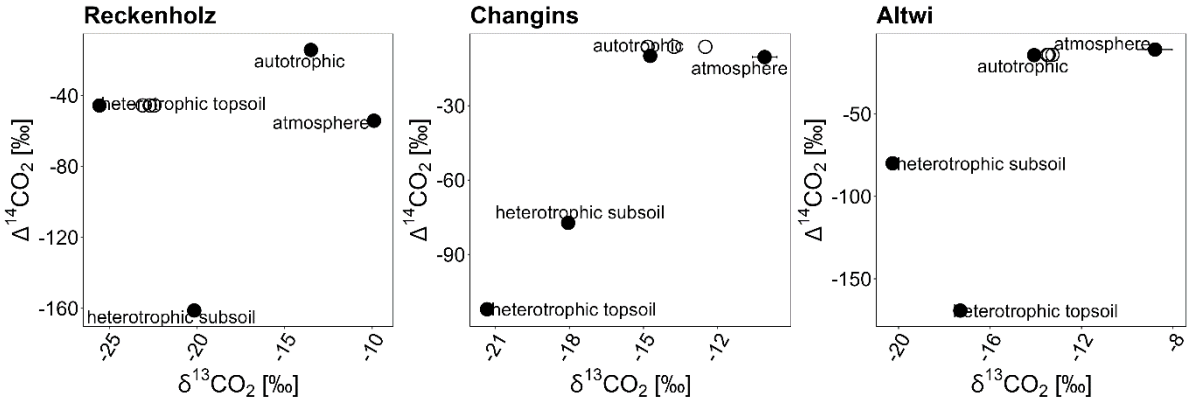

Figure S12: MixSIAR isospace plots for croplands in summer.

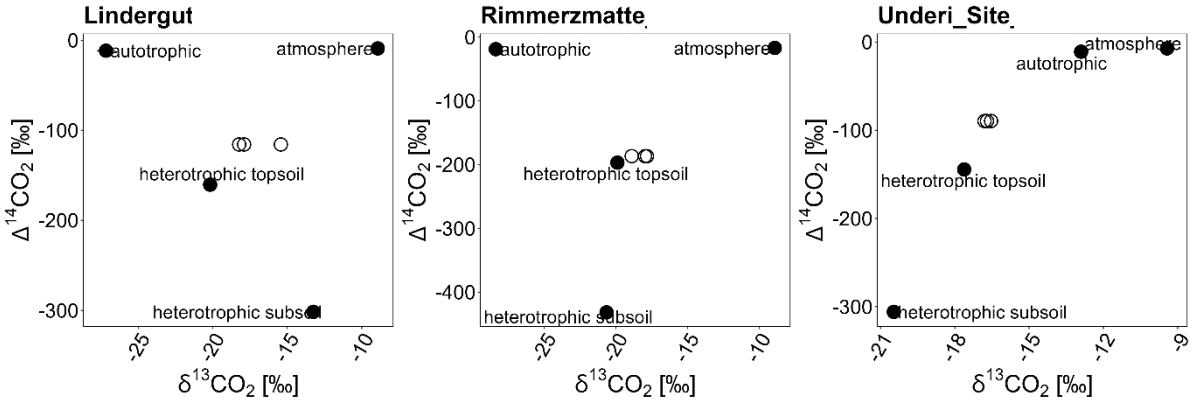

Figure S13: MixSIAR isospace plots for managed peatlands in summer.

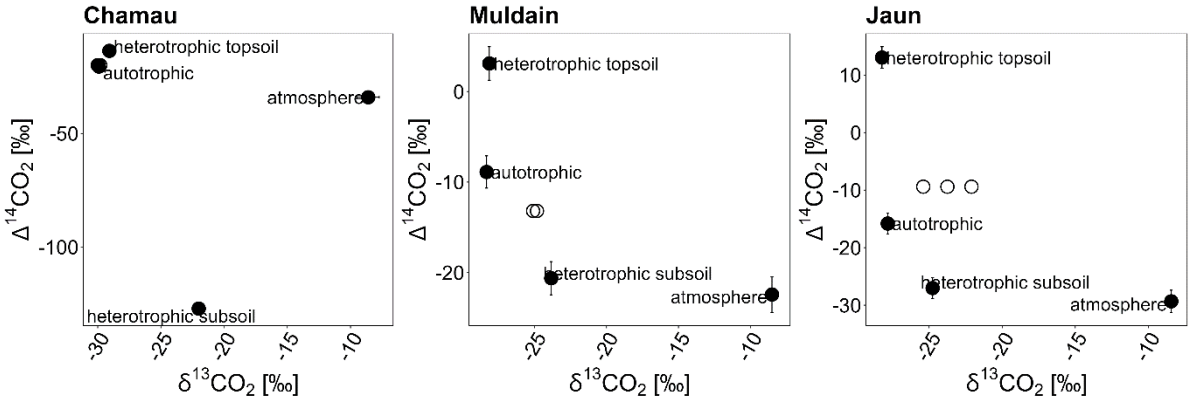

Figure S14: MixSIAR isospace plots for temperate grasslands in winter.

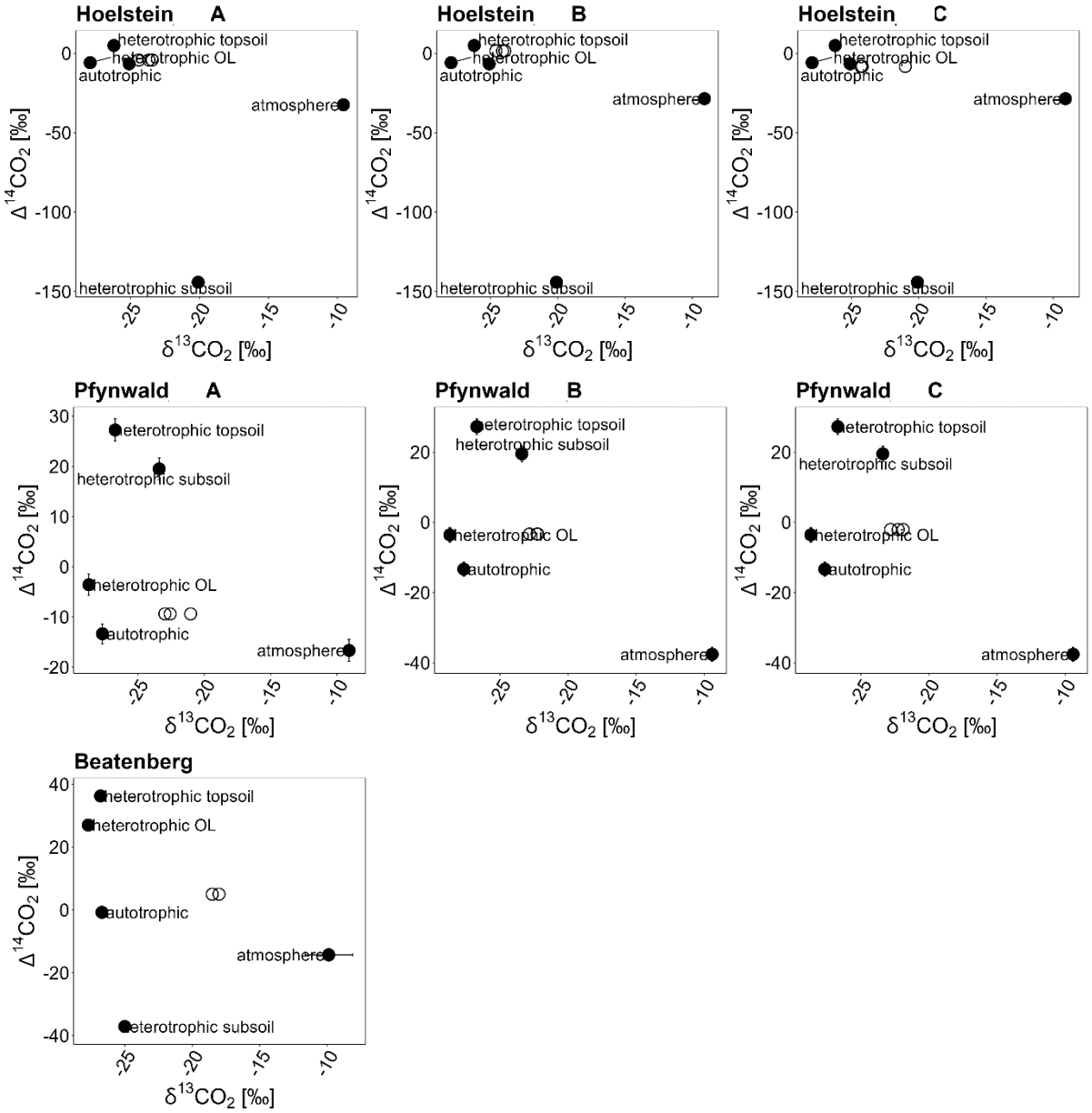

Figure S15: MixSIAR isospace plots for forests in winter. OL = organic layer.

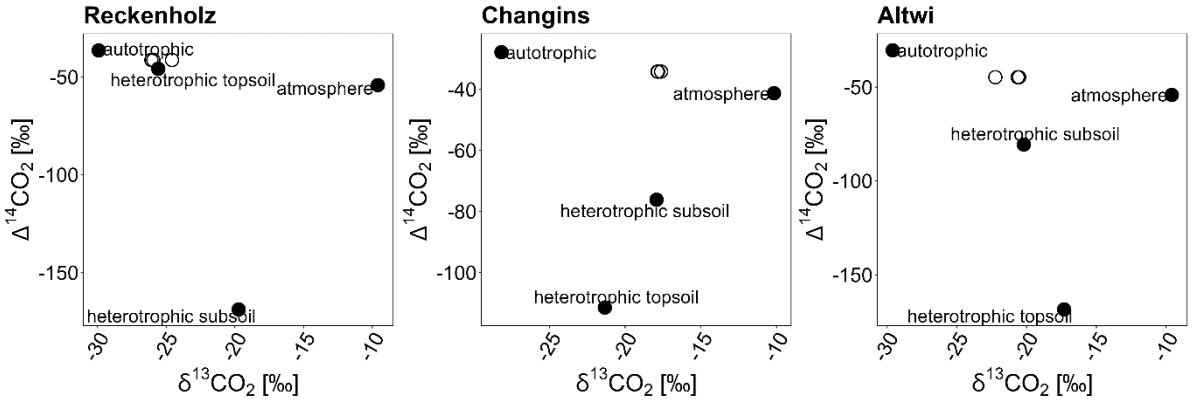

Figure S16: MixSIAR isospace plots for croplands in winter.

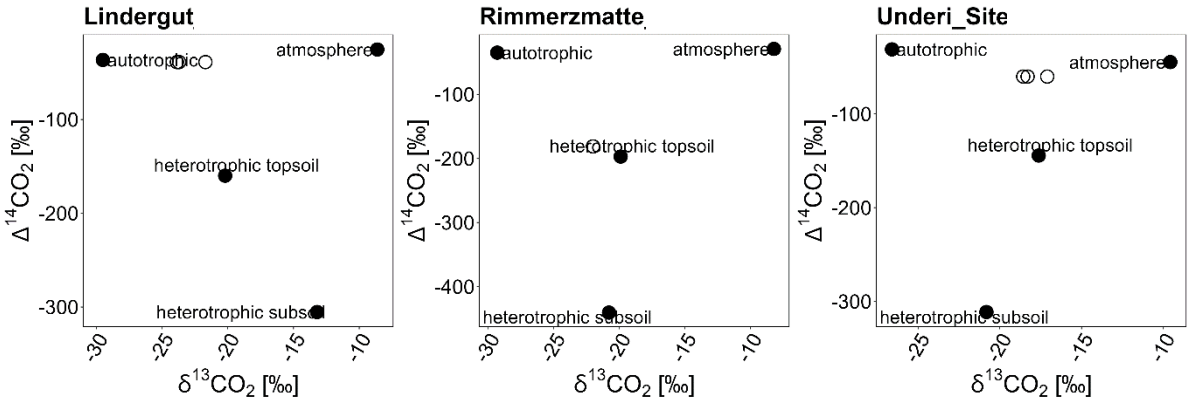

Figure S17: MixSIAR isospace plots for managed peatlands in winter.